Involvement of trabecular meshwork phagocytic suppression by sympathetic norepinephrine in nocturnal intraocular pressure rise

Keisuke Ikegami (ikegami.keisuke.910@mail.aichi-med-u.ac.jp)
Aichi Medical University https://orcid.org/0000-0001-5606-3965

Satoru Masubuchi
Aichi Medical University

Article

Keywords: CIRCADIAN RHYTHM, INTRAOCULAR PRESSURE, GLAUCOMA, SYMPATHETIC NORADRENALINE, PHAGOCYTOSIS

Posted Date: November 9th, 2021

DOI: https://doi.org/10.21203/rs.3.rs-1038571/v1

Version of Record: A version of this preprint was published at Communications Biology on April 8th, 2022. See the published version at https://doi.org/10.1038/s42003-022-03295-y.

Abstract

Intraocular pressure (IOP) is important in glaucoma development and depends on aqueous humor (AH) dynamics, involving inflow from the ciliary body and outflow through the trabecular meshwork (TM). IOP has a circadian rhythm entrained by sympathetic noradrenaline (NE) or adrenal glucocorticoids (GCs). Here, we investigated the involvement of GC and NE in AH outflow. Pharmacological prevention of inflow/outflow in mice indicated an AH outflow increase during day. Although TM phagocytosis can determine AH drainage, only NE showed a non-self-sustained inhibitory effect in phagocytosis of immortalized human TM cells. Pharmacological approach and RNA interference identified β1-adrenergic receptor (AR)-mediated cAMP-EPAC-SHIP1 signal activation by ablation of phosphatidylinositol triphosphate regulating phagocytic cup formation. Furthermore, pharmacological instillation in mice revealed the role of β1-AR-EPAC-SHIP1 pathway in nocturnal IOP rise. These suggest that IOP rhythm is partially regulated by this pathway. This first demonstration of TM phagocytosis suppression by NE could be useful in glaucoma management.

Introduction

In most organisms, multiple physiological and behavioral processes, including sleep-wake cycles, endocrine systems, and metabolism, are controlled by circadian rhythms lasting approximately 24 h. The suprachiasmatic nucleus (SCN) in the anterior hypothalamus acts as a circadian pacemaker in mammals, sensing optical information from the retina to manage the daily body rhythms of physiological and behavioral processes [1]. The SCN synchronizes most peripheral tissues and cells through various complex pathways, involving mainly the autonomic nervous system and endocrine signals [2]. Norepinephrine (noradrenaline, NE) released from the superior cervical ganglion (SCG), a part of the sympathetic nervous system, transmits circadian timing signals to the ciliary body of the eye to regulate pupil size, and to the pineal gland to regulate nocturnal melatonin synthesis [3]. Furthermore, for most peripheral tissues, glucocorticoids secreted from the adrenal glands via the hypothalamus-pituitary-adrenal axis-mediated SCN act as strong endocrine timing signals because glucocorticoid receptors (GRs) are expressed in most peripheral cell types [4].

Glaucoma is a leading cause of blindness in elderly people; however, no effective cure exists. Abnormal intraocular pressure (IOP) inside the eye, e.g. high IOP, contributes to glaucoma development and progression characterized by vision loss [5]. IOP is balanced by aqueous humor (AH) and has a circadian rhythm. In humans, nocturnal IOP increases irrespective of posture [6]. IOP is also elevated at night in nocturnal rats, mice, rabbits, and diurnal humans [7], and is controlled by the SCN in mice [8]. Nocturnal IOP is also elevated in patients with glaucoma [6,9], and the IOP rhythm undergoes phase shifts in patients with primary open-angle glaucoma and normal-tension glaucoma [9]. Normal tension glaucoma is also reported to involve an abnormal IOP rhythm [10]. Furthermore, aging desynchronizes the IOP rhythm from the sleep/wake rhythms, causing a delayed IOP rhythm in older healthy subjects [11]. Interestingly, the IOP rhythm is disrupted in night-shift workers [12]. A recent study reported that a disrupted circadian IOP

rhythm causes optic nerve damage and increases the risk of glaucoma [11]. Thus, regulation of nocturnal IOP is central to glaucoma management, and the circadian mechanism in AH dynamics is important for glaucoma therapy. However, the regulatory molecular mechanisms of this axis remain unknown.

IOP is reportedly mediated by sympathetic nerve-released NE [13,14]. However, individuals with Horner syndrome, who exhibit unilateral reduced or absent sympathetic innervation, show normal circadian aqueous-flow patterns [15]. Although adrenergic β1/2 receptors mainly mediate sympathetic nerve regulation of IOP, mice knocked out for these receptors still maintain the IOP rhythm [7]. Furthermore, many peripheral clocks in rodents are controlled by CORT [16]. Although adrenalectomy (ADX) reportedly dampens the IOP rhythms in mice under a light/dark cycle [17], the circadian aqueous-flow pattern is normal in human patients after surgical ADX [18]. These contradictory effects of NE and glucocorticoids (GCs) may explain the recent discovery demonstrating the dual pathway by which both NE and GCs transmit timing information to the eye to form the IOP rhythm in mice [19]. However, the detailed molecular mechanism remains unclear.

In AH dynamics, the non-pigmented epithelial cell (NPE) of the ciliary body participates in AH production [20]. In contrast, the trabecular outflow pathway is responsible for homeostatically regulating IOP and is regulated by the coordinated generation of AH outflow resistance mediated by the constituent cells of the trabecular meshwork (TM) and Schlemm's canal (SC) [21,22], and partially uveoscleral outflow is known to be involved in human IOP rhythm [23]. In particular, 58-70% of AH passes through the trabecular pathway in several young mouse strains [24]. Most of this resistance is believed to be generated in the inner wall region, comprising the juxtacanalicular tissue and the inner wall endothelium of the SC and its pores [25]. The mechanisms that regulate aqueous outflow resistance in normal and glaucomatous eyes remain unclear, and only a few newly approved medications target this site of resistance. To traverse through the outflow pathway, AH passes through the SC endothelial cells in transient, pressure-driven cellular outpouchings, termed "giant vacuoles" (GVs) [25]. Pores (small openings in the GVs) allow AH to enter the SC from the endothelium. Previous studies have demonstrated a reduction in the number of GVs and pores in glaucoma. However, the β1β2-adrenergic receptor (AR) antagonist timolol reduces IOP during the night only in rodents [26] but does not alter the number and size of GVs [27]. On the other hand, TM phagocytosis and phagocytosis can decrease particulate material and debris from AH, attenuating outflow resistance and contributing to IOP reduction [21]. Phagocytosis is thought to play an important role in the normal functioning of the outflow pathway by keeping the drainage channels free.

Long-term dexamethasone (Dex) treatment is known to decrease TM phagocytosis in the human eye, as well as primary TM cells [28,29], leading to increased AH outflow resistance, and ultimately, glaucoma development. In addition, NE suppresses wound macrophage phagocytic efficiency through α- and β-AR-dependent pathways [30]. However, the detailed effect of NE on TM phagocytosis has not been elucidated. Hence, this study aimed to uncover the effects of GC/NE on trabecular phagocytosis and its molecular mechanism. We addressed the effect of AH outflow on diurnal IOP changes in mice. In addition, the

efficacy of phagocytic activity by NE/GC exposure was monitored in real time using immortalized human TM cells. Pharmacological approaches and RNA interference identified the pathways involved in phagocytosis regulation. Furthermore, the role of the identified regulatory pathway in IOP rhythm regulation was assessed using pharmacological instillation in mice.

Results

AH outflow increased in the daytime in mice

To address the effects of ciliary AH-production on nocturnal increase in IOP, we injected the Na^+/K^+ATPase antagonist, ouabain, into the posterior chamber of the mouse eye at zeitgeber time (ZT) 10 (Fig. 1A). Ouabain allowed a nocturnal IOP increase (Fig. 1B), but prevented IOP increase in individual data ($p < 0.01$) (Fig. 1C), indicating the effect of AH outflow. Since AH drainage suppression from the TM by microbeads i.o. injection elevates IOP in rats [31], to identify the role of AH outflow on mouse IOP rhythm, microbeads were injected into the anterior chamber of the eye to mildly suppress the AH outflow (Fig. 1D), as previously reported [31]. After 2 weeks, IOP in bead-injected mice at ZT6 increased up to the nocturnal level (Fig. 1E), consistent with previous reports [31,32]. Day-night differences in individual IOP were arrested by bead injection (Fig. 1F), indicating a daytime decrease in IOP due to AH outflow. To confirm diurnal changes in AH drainage in the TM, we administered small fluorescent particles to the anterior chamber at ZT0 and ZT12, and subsequently observed the anterior eye extracted at ZT6 and ZT18, respectively, and measured the fluorescence intensity; here, we assumed that the particles were taken into the SC or passed through the TM (Fig. 1G). Thus, it seems plausible that AH outflow through TM/SC may be involved in the daytime decrease in IOP in mice.

Driven-output stimuli of NE may suppress phagocytosis in the TM

To investigate the effect of GC and NE on phagocytosis in the TM, we used pH-sensitive pHrodo particles to evaluate phagocytosis in real time in immortalized human TM cells (iHTMCs) (Fig. 2A). The validity of this assay was confirmed by using a control with the phagocytosis inhibitor, cytochalasin D ($p < 0.001$) (Fig. 2B). After medium changes, including NE or Dex, phagocytosis was significantly suppressed by NE (Fig. 2C, D). Continuous NE treatments dose-dependently prevented phagocytic activity in iHTMCs during 2 days of culture (Fig. 2D). Although Dex alone had no effect (Fig. 2E, F, Fig. S1A), Dex suppressed phagocytosis in a dose-dependent manner (Fig. S1B). These results indicate the importance of NE in phagocytosis.

To investigate the short-term effect of NE on phagocytic circadian rhythm and activity, we exposed iHTMC to NE for 30 min, and subsequently observed the phagocytic activity in iHTMCs in real-time for 3 days (Fig. 2G). Although we could not observe the circadian phagocytosis rhythm in the normalized fluorescence signal by control, high NE pulse stimulation immediately began to suppress phagocytosis, reaching the minimum after 9 h and showed an inhibitory effect over 24 h, while Dex stimulation did not modulate phagocytosis rhythm (Fig. 2H). These findings suggest the possibility that diurnal changes in

phagocytosis in TM may occur as a result of a driven output, but is not self-sustainable after a single NE stimulation (Fig. 2I).

β1-AR mainly attenuated phagocytosis in iHTMCs

As NE suppresses wound macrophage phagocytic efficiency through α- and β-AR dependent pathways [30], we first confirmed the gene expression of nine AR subtypes in iHTMC. Strong expression of *ADRA2A*, *ADRA2B*, *ADRA2C*, *ADRB1*, and *ADRB2* was observed, while very weak expression of *ADRA1s* and *ADRB3* (Fig. S2A) was seen, consistent with the gene expression patterns analyzed from previous single-cell RNA-seq data in human TM macrophages (Fig. S2B)[33]. To identify the AR regulating SC phagocytosis, we subsequently treated several agonists of AR (L-adrenaline, β1-AR agonists [L-NE and dobutamine], β1β2-AR agonist [isoproterenol], selective α1-AR agonist [phenylephrine], direct-acting α2-AR agonist [clonidine], and β2-AR agonists [formoterol and salbutamol]) to iHTMC for single screening. As a result, we observed the dose-dependent robust suppression of phagocytosis by L-NE, dobutamine, and isoproterenol until 3 days (Fig. 3A), even though some showed slight changes in cell viability occurred after 72 h of treatment (Fig. S3). Further detailed analysis revealed the significant suppression of phagocytosis by L-NE, dobutamine, and isoproterenol, as well as NE, but not by salbutamol (Fig. 3B), indicating the involvement of β1-AR in phagocytosis suppression. Furthermore, AR antagonists timolol (β1β2), betaxolol (β1), and ICI-118.551 (β2) tended to rescue NE-suppressed phagocytosis but not phentolamine (α-AR antagonist) in iHTMC, while antagonist alone showed no effect (Fig. 3C), indicating the involvement of β1β2-AR in phagocytosis suppression. To clarify this, we analyzed the effect of RNA interference on β1β2-AR and iHTMC phagocytosis, using siRNA against ADRB1 and ADRB2 (Fig. 3D), after verification of the inhibitory effect on gene expression (Fig. S4). Although siRNA exposure to control iHTMC did not show any changes, ADRB1 siRNA significantly increased NE-reduced phagocytic activity, but not ADRB2 siRNA (Fig. 3E). Taken together, these results present clear evidence that β1-AR mainly mediates NE effects in phagocytosis.

β1-AR mainly attenuates phagocytosis through the cAMP-EPAC pathway

β1-AR is a prototypical G protein-coupled receptor (GPCR) that preferentially couples with the stimulatory G protein G_s to induce cyclic adenosine monophosphate (cAMP) production. After dobutamine stimulation in iHTMC, we detected the downstream phosphorylation of cAMP response element binding protein (CREB), but not other Gq downstream Ca^{2+}/calmodulin-dependent protein kinase II (CaMKII), and Gi/Gq downstream protein kinase C (Fig. 4A-C), indicating the activation of the Gs-coupled GPCR. In fact, prostaglandin E2 (PGE2), which activates Gs-coupled GPCR (EP4 receptor), prevents iHTMC phagocytosis in a dose dependent manner (Fig. 4D). In addition, dose-dependent intracellular cAMP accumulation by cAMP inducers forskolin (FSK; Fig. 4E) and β1-AR agonist (L-NE and dobutamine; Fig. 4F) were observed, while betaxolol suppressed dobutamine-induced cAMP accumulation (Fig. 4G). These data demonstrate the importance of functional Gs-coupled β1-AR in HTMC phagocytosis.

cAMP binds to activate protein kinase A (PKA) or exchange proteins directly activated by cAMP (EPACs) [34]. In microglia cells and in peritoneal macrophages, myelin phagocytosis occurs with the involvement of both EPAC1 and PKA [35]. iHTMC phagocytic activity was slightly but significantly reduced by cAMP inducers (FSK and IBMX) and cAMP analogs, such as the PKA activator Sp-cAMP and the Epac/PKA activator 8-CPT-cAMP (Fig. 4H). To clarify the importance of PKA and EPAC in phagocytosis, RNA interference against *PRKACA, RAPGEF3*, and *RAPGEF4*, encoding PKA, EPAC1, and EPAC2, respectively, insufficiently but significantly rescued β1-AR -mediated suppression of iHTMC phagocytosis (Fig. 4I). Furthermore, blocking of PKA and EPAC1/2 by antagonists (KT5720 and ESI09, respectively) dose-dependently rescued this effect (Fig. 4J), indicating the involvement of both pathways. NE and isoproterenol suppress the phagocytosis of microglia cells via EPAC activation [36], while these findings clearly suggest that Gs-coupled β1-AR modulates iHTMC phagocytosis via PKA and EPAC.

NE decrease PIP3 through SHIP activation via EPAC and PKA.

PI(3,4,5)P3 (PIP3) is necessary for phagocytosis [37] (Fig. 5A). To verify the role of PIP3 in iHTMC phagocytosis, the PIP3 antagonist PITenin-7 administration dose-dependently and significantly suppressed the phagocytic activity of iHTMC (Fig. 5B). PI3K produces PIP3 from PI(4,5)P2 [38](Fig. 5A). Class I PI3K has four isoforms: α, β, γ, and δ. PI3Kγ, but not α, β, and δ, modulates the phagocytosis of microglia, which is suppressed by cAMP-mediated EPAC activation [39]. When we exposed LY294002 (broad-spectrum inhibitor of PI3Kαβδ) and CAY10505 (selective PI3Kγ inhibitor) to iHTMC, only CAY10505 slightly but significantly restrained phagocytosis (Fig. 5C). Furthermore, we detected a decrease in PIP3 levels by dobutamine (Fig. 5D). These results clarified that β1-AR-mediated PIP3 modulates phagocytosis in iHTMCs.

In macrophages, PKA does not inhibit phagocytosis, whereas Epac1 exerts an inhibitory effect mainly through activation of tyrosine phosphatase SHIP1 [40] (Fig. 5A). SHIP1 converts PIP3 to PI(3, 5)P2[38] (Fig. 5A). In addition, activated SHIP1 has been reported to dephosphorylate PTEN, catalyzing PIP3 in macrophages [40], and single-cell RNA-seq analysis has suggested that both SHIP1 and PTEN are expressed in human TM macrophages [33]. In fact, exposure of iHTMC with PKA and EPAC inhibitors improved the PIP3 suppression efficacy of dobutamine (Fig. 5D). In addition, the PTEN inhibitor bisperoxovanadium (pyridine-2-carboxyl) [bpV(pic)] and SHIP1 inhibitor 3-a-aminocholestane (3AC) also improved this efficiency (Fig. 5D), indicating the involvement of the β1-AR-signaling pathway in PIP3 reduction. Based on the results presented above, we next performed western blot analysis of SHIP1 phosphorylation to determine the effects of β1-AR-mediated PKA and EPAC signaling in iHTMCs. Dobutamine induced the phosphorylation of SHIP1, which was prevented by EPAC inhibition, but not PKA inhibition (Fig. 5E), indicating the importance of β1-AR-mediated SHIP1 activation through EPAC.

As PIP3 stimulates AKT and ERK1/2 signaling to modulate phagocytosis in macrophages [40], we next verified the effect of the signaling pathway of NE on AKT/ERK1/2 phosphorylation (Fig. 5A, F). Dobutamine cleanly inhibited their phosphorylation, which recovered significantly with EPAC inhibitors,

but not with PKA inhibitors (Fig. 5F). AKT/ERK1/2 phosphorylation suppressed by dobutamine was upregulated by PTEN and SHIP1 inhibitors (Fig. 5F). These results indicate the involvement of SHIP/PTEN-reduced PIP3 in the EPAC-mediated suppression of AKT/ERK activation. Furthermore, when we monitored the effect of PTEN and SHIP1 inhibitors on the phagocytosis suppression effect of dobutamine, only SHIP1 inhibitors dose-dependently rescued it up to the near control level, but no effect was seen for the PTEN inhibitor or the antagonist alone (Fig. 5G). These results suggest that, at least *in vitro,* β1-AR-mediated SHIP1 activation through EPAC reduces PIP3 to suppress phagocytic cup formation.

Nocturnal activation of the β1-AR-EPAC-SHIP1 pathway enhanced IOP in mice

Based on the results presented above, we next performed immunohistochemical analysis to determine the localization of Adrb1 and Ship1 in the mouse eye (Fig. S6). This demonstrated the colocalization of Adrb1 and Ship1 within the enthothelial cells in the SC and the non-pigmented epithelial cells in the ciliary body (Fig. S6), providing evidence of the existence of the β1-AR-Epac-Ship1 system in mice.

Since NE released from the SCG has a circadian rhythm with nocturnal increase in rodents [41], which seems to also be true in humans, a nocturnal increase of NE in TM may cause IOP increase by inhibiting phagocytosis in the TM. To validate this hypothesis, we gave mice inhibitor instillation at ZT10 and measured IOP in the night (ZT15) (Fig. 6A). First, the β1-AR antagonist slightly blocked the nocturnal IOP increase (Fig. 6B). Furthermore, instillation with EPAC and SHIP1 inhibitors significantly suppressed the nocturnal IOP increase (Fig. 6B) and also in individual level ($p < 0.01$); however, the PKA inhibitor did not show this effect (Fig. 6C), suggesting the role of the β1-AR-EPAC-SHIP1 pathway in nocturnal IOP increase. As we demonstrated the possibility of a driven-output phagocytic activity (Fig. 2), we next measured day-night changes in IOP 1 day before and after instillation to verify whether SHIP1 inhibition suppresses IOP rhythm in a self-sustainable manner (Fig. 6D). Interestingly, SHIP1 inhibition by single instillation did not reveal any inhibitory effect on nocturnal IOP increase at next day after instillation (Fig. 6D), providing evidence of driven-output IOP enhancement by nocturnal NE (Fig. 6E).

To verify the IOP inhibitory effects of drugs on β1-AR-mediated IOP regulation *in vivo*, we then gave mice dobutamine instillation at ZT4 to increase the IOP (Fig. 6F). Five hours after administration, the IOP was significantly and clearly enhanced (Fig. 6G, H). Importantly, preinstillation with a β1-AR antagonist prevented this increase (Fig. 6G, H), confirming that IOP enhanced the effect of β1-AR. To determine the role of EPAC and SHIP1 in this effect, we blocked dobutamine-activated PKA, EPAC, or SHIP1 (Fig. 6G, H). Preinstillation of EPAC and SHIP1 inhibitors significantly suppressed IOP increase (Fig. 6G, H) and prevented IOP increase in individual data ($p < 0.01$); however, the PKA inhibitor did not show this effect (Fig. 6H), indicating the importance of the β1-AR-EPAC-SHIP1 pathway in IOP regulation. Taken together, these findings revealed that nocturnal NE suppresses phagocytosis-mediated AF outflow through β1-AR-EPAC-SHIP1 activation, leading to an increase in the IOP at night (Fig. 6I).

Discussion

Previous studies have indicated that sympathetic NE and adrenal GC transmit circadian timing signals to the eye to generate IOP [19]. However, the involvement of NE and GC in TM phagocytosis contributing to IOP regulation remains unknown [42,43]. In this study, we found that suppression of AH drainage in mice may partially contribute to diurnal IOP reduction. In addition, we first demonstrated that driven-out suppressed TM phagocytosis by NE *in vitro*, which is regulated by β1-AR-cAMP-EPAC-SHIP1 activation. cAMP binds to PKA and EPAC1/2 [34], which are both involved in myelin phagocytosis in microglia cells [35] and macrophages [40,44]. Long-term Dex exposure decreased TM phagocytosis in the human eye and primary TM cells [28,29], and GC alone showed no effect up to 3 days after exposure (Fig. 2). We further identified β1-AR -suppressed TM phagocytosis by silencing PIP3-AKT or -ERK signaling. Although it is known that NE suppresses macrophage phagocytosis [30], and PIP3 stimulates AKT and ERK1/2 signaling to modulate phagocytosis [37,40], the connection between NE and PIP3-triggered phagocytosis remains unclear. We demonstrate success, for the first time, in connecting the signaling pathway: PIP3 reduction through the cAMP-EPAC-SHIP1 pathway. SHIP1 activation by cAMP-EPAC suppresses phagocytosis in macrophages [40] by decreasing PIP3 [38]. These results support our hypothesis that cAMP-EPAC-SHIP1 activation prevents phagocytic cup formation by decreasing PIP3 (Fig. 6l).

We further found a slight but significant involvement of PKA in β1-AR-mediated phagocytosis and PIP3 reduction (Fig. 5). Although we demonstrated TM phagocytosis through PI3Kγ, PI3Kγ may modulate phagocytosis not only by EPAC activation [39], but also by PKA activation. PKA activation can cause the conversion of Gαs to Gαi in β2-AR in HEK293 cells [45]. It is possible that β1-AR-mediated TM phagocytosis inhibition may be mediated by PKA-suppressed Ras homolog gene family A (RHOA), which contributes to phagocytosis. RHO is a member of the small GTPases CDC42 and RAC1 [37] associated with the cytoskeleton. RHO-kinase inhibitors enhance the drainage of AH into the SC to reduce IOP, and RHOA blocking prevents nocturnal IOP elevation [46]. In fact, RHOA activation decreases TM phagocytosis [47]. The involvement of these small GTPases in NE-mediated TM phagocytosis remains to be elucidated.

In general, β-AR blockers, including betaxolol, effectively reduce IOP by decreasing AH inflow in patients [48]. Several studies have demonstrated the opposite effect of the sympathetic role in AH outflow. β-AR may be involved in the increase of AH outflow by reducing the size of cells in the TM [49]. Continuous electrical stimulation of the cervical sympathetic nerve decreases IOP only during 1 h [50]. However, since these findings suggest the importance of β2-AR, β1-AR may contribute to nocturnal AH outflow resistance. β1-AR stimulates cAMP production only through Gαs, while β2-AR may also couple to the Gαi protein, which enhances the PIP3/Akt pathway in cardiomyocytes [51] and HEK293 cells through PKA activation [45]. Although the differences in the human TM or eye remain unclear, the strong inhibitory effect of β1-AR and weak inhibition of β2-AR in the present study may be the cause of the differences. Furthermore, primary open-angle glaucoma (POAG) involves a greater increase in IOP at night than during the day [10]. Interestingly, a recent study revealed that the β1-AR antagonist betaxolol, a clinically used medication for the treatment of ocular hypertension and chronic open-angle glaucoma, is the top compound most opposed to POAG signatures calculated by microarray database analysis [52].

Furthermore, in the TM of the POAG donors, the cAMP signaling pathway and CREB were activated [53], while ERK phosphatase activity was downregulated [54], consistent with the NE-activated cAMP signaling pathway and suppressed ERK activation in the present study. It is certain that further understanding of this pathway is necessary to fully explain the complex cellular mechanisms by which occupancy of specific ARs regulates AH dynamics, which may contribute to the establishment of chronotherapy.

Betaxolol decreased the β1-AR-mediated IOP increase, while slightly prevent nocturnal IOP (Fig. 6). This slight effect may be caused by the maintenance of β2-AR- or GC-mediated AH production in the NPE of the ciliary body [19]. β-AR1/2 double knockout mice maintain this IOP rhythm [7]. It can be seen that the contribution of β1-AR-mediated circadian rhythm of AH resistance for IOP rhythm formation is not very high. Ouabain instillation did not completely arrest the IOP rhythm (Fig. 1), indicating the involvement of not only the outflow rhythm in IOP rhythm generation, but also the ciliary carbonic anhydrase (CA) in HCO_3^- production [55]. DEX stimulation increases CAII expression in the mouse brain [56]. Soluble adenylyl cyclase has been reported to be activated to produce cAMP by CA-converted HCO_3^- [57]. Ciliary CA may produce a GC/NE-mediated AH rhythm. In contrast to the slight effect of betaxolol on nocturnal IOP increase, inhibitors of EPAC or SHIP1 dramatically arrested nocturnal IOP increase. This could be explained by two hypotheses: the inhibitors enhance the AH outflow by acting on pathways other than TM phagocytosis, such as GV in the endothelial cells of the SC, or AH inflow, that is, Na^+/K^+ATPases and CA in the NPE of the ciliary body. In fact, single-cell RNA-seq analysis has suggested that *RAPGEF3*, *RAPGEF4*, and *SHIP1* are expressed in human SC endothelial cells [33]. We further detected SHIP1 expression in NPE. Since instillation of these inhibitors did not suppress the dobutamine-induced IOP increase to below the normal level, the latter possibility is more likely, although it may not be detected well because the IOP level is usually quite low.

TM phagocytosis rhythm seems to be directly driven by NE, but not by an autonomous rhythm (Fig. 2, 6). This regulatory pathway is consistent with β1-AR-mediated circadian regulation of the pineal gland [58]. In our previous report, NE instillation generated a transient IOP increase within 1 day, but not the day after instillation [19]. It may be possible to partly explain not only the AH production rhythm, but also the NE-mediated driven-out rhythm of AH outflow resistance. The physiological importance of the driven-output rhythm and circadian clock in the TM remains unclear. Considering the role of IOP in maintaining the camera function of the eye, the strength of being able to respond flexibly to acute stress and fluctuations may be important in adjusting IOP.

In the present study, a pharmacologically high dose of Dex triggered the inhibition of TM phagocytosis only with NE, but Dex alone had no effect even under high doses, indicating the existence of the dual regulatory pathway, suggesting that NE is a necessary condition for GC function in the TM. Although some previous studies have demonstrated that high doses of GCs (10^{-6} to 10^{-5} M) suppress phagocytosis of neutrophils [59] and TM (10^{-7} to 10^{-6} M) [28,29], GCs combined with β2-AR have no effect on neutrophil phagocytosis [59]. Since the physiological dose of Dex (10^{-9} M) did not alter phagocytosis in iHTMCs (Fig. S1), the physiological implications of these dual regulatory pathways remain unknown.

However, both β-adrenergic signaling and glucocorticoids are mediators of SCN timing signals in osteoblasts [60]. Interactions between the sympathetic nervous system and GCs have also previously been reported. In particular, GC transcriptionally modulates β2-AR expression by modulating GC-response elements (GREs) on the promoter [61]. Interestingly, GCs rapidly activate cAMP production via Gαs to initiate non-genomic signaling, which contributes to one-third of their canonical genomic effects [62]. Thus, in TM, Gs-bound GR may enhance the β1-AR-Gs signal to suppress phagocytosis. GC also binds to the TM and endothelial cells in the SC in humans [63], and its receptor localizes in mouse TM [19]. β2-AR acts on human TM and SC [49], and β1-AR is expressed in mouse TM, SC, and human TM cells (Fig. 3, Fig. S2, Fig. S6). Thus, the interaction between GCs and NE can generate an appropriate AH drainage rhythm.

Our study has several inherent limitations. First, although we provide a model of IOP induction in nocturnal NE, the circadian rhythm of NE released from SCG in humans remains unclear. Although GC secretion peaks at the light offset [64], and NE is released with a nocturnal peak from the SCG in rodents [65], GC rhythms are anti-phasic but not SCG-NE in diurnal animals [65,66]. Nocturnal NE release from SCG generally stimulates melatonin synthesis in humans, as well as in other mammals [67]. In human, β-blockers inhibit nocturnal melatonin levels [68], and suppress IOP increase during late night to morning [69]. Furthermore, in nocturnal rabbits, β-blockers suppress IOP increases only at night [26]. These results indicate the involvement of nocturnal NE release from the SCG in regulating the IOP rhythm. Second, we cannot fully explain the differences in IOP rhythms in diurnal and nocturnal animals. The IOP rhythm peaks early at night in nocturnal animals [7], while in healthy humans, it appears to be elevated during the night and peaks from late night to early morning [6,9]. In phasic SCG-NE and anti-phasic GC, the action of both factors in IOP increase may be able to explain such differences. Third, we explain AH outflow from the AH resistance rhythm by NE. However, the involvement of other determinants of outflow in circadian AH outflow remains unclear. IOP-independent uveoscleral outflow to the ciliary muscle may explain this paradox (Fig. 6I). In mice, 30-42% of AH passes through the uveoscleral pathway [24]. To understand the AH dynamic rhythm completely, these determinants need to be elucidated.

Taken together, these results suggest a potential circadian role for NE in the modulation of phagocytosis and AH outflow resistance by TM contributing to the IOP rhythm. Currently available drugs lower IOP mainly by diminishing the inflow of AH or enhancing drainage via the uveoscleral pathway. Although the TM accounts for most outflow and is the major site of AH outflow resistance [24,70], until the approval of the ROCK inhibitor, no clinically administered drug had a direct effect on the TM. The major reason for this is a poor understanding of the mechanisms underlying its function. In the present study, we provide the possibility of therapeutic drug development targeting TM using NE-mediated resistance to AH outflow. In addition, although we demonstrated the GC/NE interaction in TM phagocytosis, the synergistic regulatory mechanism of GC in the presence of NE in AH dynamics remains unknown. Since non-genomic signaling may also contribute to this mechanism [62], further understanding of time-dependent efficacy and the duration of GC and NE on AH inflow and outflow will lead to a complete elucidation of the regulatory mechanisms of IOP rhythm. Although new therapeutics with new mechanisms, such as

chronotherapy, are urgently needed for glaucoma treatment, the development of multiple types of drugs using this interaction could be very useful for glaucoma treatment in the future.

Methods

Animals

Five-week-old male C57BL/6JJmsSlc mice (N =130; Japan SLC Inc., Shizuoka, Japan) were purchased and housed in plastic cages (170 W × 240 D × 125 H mm, Clea, Tokyo, Japan) under a 12-h light (200 lx of fluorescent light) / dark cycle (12L12D, 0800 light ON, 2000 light OFF), maintained at a constant temperature (23 ± 1 °C). Food (CE-2; CLEA) and water were provided *ad libitum*. All animal experiments were approved by the Committee of Animal Care and Use of the Aichi Medical University. All experimental procedures were conducted in accordance with the institutional guidelines for the use of experimental animals.

IOP measurement

IOP measurements were performed using a tonometer (Icare TonoLab, TV02; Icare Finland Oy, Espmoo, Finland), as previously reported [8,19]. All mice were kept under 12L12D conditions for more than 2 weeks before IOP measurements. Unanesthetized mice were gently held using a sponge. IOPs were measured during the light phase under light (200 lx) conditions and during the dark phase under dim red-light conditions. To analyze nocturnal IOP increase, IOP was obtained by measuring the IOP at zeitgeber time (ZT) 10 and ZT15. ZT0 (0800) was defined as the time of light ON. For diurnal changes in IOP, IOP was measured at ZT6 and ZT15 2 weeks after bead injection. For the analysis of dobutamine-mediated IOP induction, IOP was measured before drug instillation at ZT4 and measured at ZT9.

Intraocular injection and detection of fluorescence particles

To investigate the effect of AH inflow on nocturnal IOP increase, mice were anesthetized by isoflurane inhalation (2%; WAKO, Saitama, Japan), supplemented with topical proparacaine HCl (0.5%; P2156, Tokyo, Tokyo Chemical Industry [TCI]), and were treated with an intraocular injection of an Na+/K+ATPase inhibitor ouabain (100 μM / 0.1% DMSO phosphate-buffered saline [PBS], 2 μL) into the right eye with a 34-gauge needle (0.18 × 8 mm, Pasny; Unisis) connected to a Hamilton syringe at ZT10. To precisely control the small volume (3 μL) of anterior chamber injection, 3 μL PBS (0.1% DMSO) was injected into the left eye with a 34-gauge needle connected to a Hamilton syringe.

For microbead injection to prevent AH outflow, mice were anesthetized by isoflurane inhalation (2%; WAKO, Japan), supplemented with topical proparacaine HCl. IOP elevation was induced unilaterally in adult C57BL/6J mice by injection into the anterior chamber of 3 μL of 1/10 diluted fluosphere polystyrene microspheres (15 μm, yellow-green fluorescent, F8844, Invitrogen, Carlsbad, CA) of the right eye with a 34-gauge needle connected to a Hamilton syringe. Microbeads were then resuspended in PBS at 5.0×10^6

beads/mL. To precisely control the small volume (3 μL) of anterior chamber injection, 3 μL PBS was injected into the left anterior chamber with a 34-gauge needle connected to a Hamilton syringe.

To visualize the AH outflow in the SC, mice were anesthetized by isoflurane inhalation (2%; WAKO, Japan), supplemented with topical proparacaine HCl, and were treated with an intraocular injection of 3 μL of carboxylate-modified microspheres (0.5 μm, yellow-green fluorescent, 2% solids, F8813, Invitrogen) at ZT0 and ZT12. After 6 h, the injected mice were anesthetized, and their anterior eyes were extracted and fixed in 4% paraformaldehyde (26126-25, Nakarai) / PBS for 5 min. After being washed with PBS, anterior eye cups were placed in Hanks' Balanced Salt Solution (HBSS; 082-08961 WAKO) in a 96-well microplate to observe the fluorescence from the bottom by digital fluorescent microscope Dino-Lite Edge M Fluorescence TGFBW (Opto Science Inc.), and the fluorescence intensity (525 nm) was measured using a microplate reader SpectraMax M5 (Molecular Devices).

iHTMC culture

The immortalized human TM-SV40 cell line (iHTMC) derived from primary human SC and TM region was purchased from Applied Biological Materials Inc. (T-371-C, ABM Inc., Richmond, BC, Canada) and cultured in TM cell medium (6591, Sciencell, Carlsbad, CA, USA) supplemented with 10% fetal bovine serum (0010, Sciencell), 1% growth supplement (TMCGS, 6592, Sciencell) and 1% penicillin/streptomycin (0503, Sciencell) in type I collagen-coated 100-mm dish (3020-100, IWAKI, Japan). Experiments were performed in type I collagen-coated plates. Upon reaching confluence, iHTMCs were split 1:4 using 0.05% trypsin/PBS. Cell viability was determined using trypan blue (0.4%) exclusion.

Phagocytosis assay and drug treatment

For phagocytosis assay, iHTMCs (T0371, abm) were plated in collagen I-coated 96-well microplates (4860-010; IWAKI) at a density of 5.0×10^3 cells/well in trabecular meshwork cell medium (TMCM) supplemented with 1% penicillin/streptomycin and growth factors (6591; Sciencell). To measure phagocytosis, pHrodo Green Zymosan Bioparticles (P35365; ThermoFisher) were resuspended in PBS and vortexed to disperse. After 90% confluence, the medium was removed by aspiration, and 100 μL of serum-free TMCM was immediately added. After 24 h, the medium was replaced with serum-free TMCM containing pHrodo Zymosan (2.5 μg / well) in the presence of several kinds of drugs, and the plate was placed in the Incucyte ZOOM instrument (Essen Bioscience, Ann Arbor, MI, USA), installed in a 5% CO_2 incubator at 37 °C. Each well was imaged at 3 points, every 0.5 h or 1 h for more than 72 h using the phase and green fluorescence channels and the 10× objective. No pHrodo Zymosan was used for fluorescent control using background fluorescent intensity because of autofluorescence in TMCM, and vehicle control included 0.1% DMSO. At the end of the experiment, the fluorescence intensity at each time point in each well was measured using the IncuCyte ZOOM 2015A software (Essen Bioscience). To perform the detailed analysis of the pulse stimulation, we calculated the difference from the control. We calculated the average daily fluorescence intensity normalized to that of the control DMSO treatment group to show statistical changes. The phagocytosis assay was independently repeated three times

using four biological replicates. Data were combined and averaged, and the standard error was calculated.

Drug treatment

For the phagocytosis assay, iHTMCs were simultaneously treated with (−)-NE (0.1, 1, and 10 μM; S9507, Selleck) and/or dexamethasone (Dex; 0.1, 1, and 10 μM; 11107-51, Nakarai Tesk) and pHrodo Zymosan. To confirm the phagocytic activity in iHTMC, we treated to iHTMCs with the phagocytosis inhibitor Cytochalasin D (0.01 nM; 11330, Cayman). For detailed analysis of pulse stimulation, serum-free TMCM including NE (1, 10, and 100 μM) or Dex (0.1, 1, and 10 μM) were added to iHTMC for 30 min. After being washed with TMCM, pHrodo zymosan-containing TMCM was added to iHTMC. For analysis of effect of agonists on phagocytosis, we treated several kinds of agonists for AR agonist L-Adrenaline (A0173, TCI), β1-AR agonists (L-Noradrenaline Bitartrate Monohydrate [L-NE, A0906, TCI] and dobutamine hydrochloride [15582, Cayman], β1β2-AR agonist [Isoproterenol Hydrochloride (I0260, TCI), selective α1-AR agonist [L-Phenylephrine (P0395, TCI)], direct-acting α2-AR agonist [Clonidine HCl (038-14291, WAKO)], β2-AR agonist [Formoterol fumarate hydrate (F0881, TCI)], short-acting β2-AR agonist (Salbutamol Hemisulfate [S0531, TCI]), PGE2 (0.1, 1, and 10 μM; P1884, TCI), cAMP inducers (Forskolin [10 μM FSK; F0855, TCI] and 3-Isobutyl-1-methylxanthine [10 μM IBMX; 095-03413, WAKO]), cAMP analogs as PKA activator Sp-cAMP (10 μM; 14983, Cayman) and as Epac/PKA activator 8-CPT-cAMP (10 μM; 12011, Cayman) to iHTMC. For analysis of antagonists for ARs, NE (5 μM) were simultaneously added with antagonists; β1β2-AR antagonist Timolol Maleate (1, 10, and 100 μM; T2905, TCI), β1-AR antagonist Betaxolol hydrochloride (1, 10, and 100 nM; B4474, TCI), β1-AR antagonist ICI-118.551 hydrochloride (0.01, 0.1, and 1 μM; HY-13951, MCE), α2-AR antagonist phentolamine mesylate (100 μM; P1985, TCI), PKA inhibitor KT5720 (0.001, 0.01, 0.1, and 1 μM; 10011011, Cayman), EAPC1/2 inhibitor ESI09 (0.1, 1, 10, and 100 μM; 19130, Cayman), PTEN inhibitor bpV (pic) (0.001, 0.01, 0.1, and 1 μM; SML0885, Sigma-Aldrich), and 3α-aminocholestane (0.01, 0.1, 1, and 10 μM; 3AC; HY-19776, MCE). To regulate PIP3 content, we treated iHTMC with the PIP3 antagonist PITenin-7 (0.01, 0.1, 1, and 10 μM; 524618, Calbiochem), PI3Kαβδ inhibitor LY294002 (70920, Cayman), and selective PI3Kγ inhibitor CAY10505 (HY-13530, MCE).

Western blot analysis

Western blot analysis was performed as previously our report [71]. Protein extraction was performed using cell lysis buffer (9803, Cell Signaling Technology, Tokyo, Japan) containing protease inhibitor cocktail (P8340, Sigma) and phosphatase inhibitor cocktail 1 (P2850, Sigma) according to the manufacturer's instructions. Total protein transferred to the PVDF membrane was detected using EzStainAQua MEM (WSE-7160, ATTO) and used for normalization. After destaining, membranes were incubated with the following primary antibodies: rabbit monoclonal antibodies against phospho-CREB (Ser133) (1:1000; 9198, Cell Signaling Technology), CREB (1:1000; 9192, Cell Signaling Technology), Akt (pan) (C67E7) (1:1000; 4691, Cell Signaling Technology), and rabbit polyclonal antibody against phospho-PKCα/βII (Thr638/641) (1:1000; 9375, Cell Signaling Technology), phospho-Akt (Thr308) (1:1000; 9275, Cell

Signaling Technology), phosphor-CaMKII alpha (Thr286) (1:1000; ab5683,abcam), ERK1 / ERK2 (1:1000; A16686, ABclonal), phospho-ERK1(T202/Y204) /ERK2(T185/Y187) (1:1000; AP0472, ABclonal), INPP5D (SHIP1) (1:1000; A0122, ABclonal), phosphor-INPP5D (Tyr1021) (1:1000; PA903060, CSB), and mouse monoclonal antibody against CaMKIIα/β/γ/δ (G-1) (1:500; sc-5306, Santa Cruz Biotechnology). Membranes were washed and then incubated with HRP-conjugated goat polyclonal antibody against mouse and rabbit IgG (1:10,000; 7074, Cell Signaling Technology). Chemiluminescent images were detected using an Amersham Imager 600 (Cytiva Lifescience).

cAMP measurement

cAMP measurements were performed with a homogeneous TR-FRET immunoassay using the LANCE cAMP Detection Kit (AD0262, PerkinElmer, USA), according to the manufacturer's instructions (PerkinElmer). After confluence, iHTMCs in collagen I-coated 96-well microplates (4860-010; IWAKI) were washed with PBS (0.2 g/L EDTA), and then washed with stimulation buffer (HBSS, 5 mM HEPES, 0.5 mM IBMX, and 0.01% BSA at pH 7.4). After aspiration, iHTMC was added to 10 µL of tested compounds with FSK (0.001, 0.01, 0.1, and 1 µM), L-NE (0.01, 0.1, 1, and 10 µM), and dobutamine (0.001, 0.01, 0.1, 1, and 10 µM), and 10 µL of Alexa Fluor 647 anti-cAMP antibody diluted with stimulation buffer. The cells were then stimulated for 60 min at room temperature. The antagonist response analysis was performed using L-NE or dobutamine as the reference agonist. To analyze the antagonist effect on β1-AR, the β1-AR agonist L-NE or dobutamine was used at submaximal concentrations (10 µM and 1 µM, respectively) to stimulate cAMP accumulation. These agonists and the β1-AR antagonist betaxolol (0.05, 0.5, 5, and 50 µM) were simultaneously added. After incubation, the reaction was stopped, and cells were lysed by the addition of 20 µL working solution (10 µL Eu-cAMP and 10 µL ULight-anti-cAMP), and incubated for 1 h at room temperature. The TR-FRET signal was read using a microplate reader SpectraMax M5 (Molecular Devices). cAMP concentrations were determined using GraphPad Prism software (version 6.0; GraphPad Software Inc., San Diego, CA).

Small interfering RNA knockdown

iHTMCs were seeded in quadruplicate into collagen I-coated 96-well microplates (4860-010; IWAKI) at a density of 5.0×10^3 cells/well with serum-free TMCM (1% penicillin/streptomycin; #6591; Sciencell). Twenty-four hours later, cells were transfected with 0.04 µM Accell SMARTpool siRNA against *ADRB1*, *ADRB2*, *RAPGEF3*, *RAPGEF4*, *and PRKACA* (Table EV1, Dharmacon), Accell *GAPDH* pool-human siRNA (D-001930) as a positive control, and Accell Non-targeting pool siRNA (D-001910) as a negative control using 100 µL Accell Delivery Media (B-005000-100; Dharmacon) according to the manufacturer's instructions. Twenty-four hours later, NE (1 µM; 20 µL/well) or 0.1% DMSO with PBS containing pHrodo Green Zymosan Bioparticles (2.5 µg / well; P35365) were added. After 24 h of exposure to siRNA, total RNA was extracted and purified as described above for knockdown confirmation by qPCR.

Drug instillation

Drug instillation was performed as described in our previous report [19]. Unanesthetized 8-week old male mice were used in this study. For nocturnal IOP increase analysis, mice were instilled with a single drop (30 µL) of betaxolol (100 µM / 0.1% DMSO PBS), KT5720 (100 µM), ESI09 (100 µM), 3AC (1 mM), SHIP1 inhibitor K118 (1 mM; B0344, Echelon Biosciences), and bpV (pic) (100 µM) at ZT10 using a micropipette into bilateral eyes, and IOP was measured at ZT15. To analyze the inhibitory efficacy of dobutamine-induced IOP increase, the above antagonists were preinstillated at ZT4, and then, after 10 min, a single drop of dobutamine (100 µM / 0.1% DMSO PBS) was added. During instillation, the mice were gently restrained with the necks held back.

PIP3 extraction and quantification

PIP3 measurements were performed using ELISA kits (Echelon Biosciences, K-2500s) according to the manufacturer's instructions. iHTMCs were seeded at a density of 1.2×10^6 cells/collagen I coated 6 well dish (IWAKI). After 14 h of treatment with dobutamine (1 µM) with or without agonists, KT5720 (10 µM), ESI09 (1 µM), bpV (pic) (1 µM), and 3AC (10 µM), the media were removed by aspiration and 1 mL of ice-cold 0.5 M tricarboxylic acid (TCA) was immediately added. Cells were scraped, transferred into a 1.5-mL tube on ice, and centrifuged at 3,000 rpm for 7 min at 4°C. The pellet was resuspended in 5% TCA/1 mM EDTA (0.5 mL), vortexed for 30 s, and centrifuged at 3,000 rpm for 5 min at room temperature. After discarding the supernatant, this washing step was repeated once more. Next, neutral lipids were extracted by adding 0.5 mL of MeOH:$CHCl_3$ (2:1) and continuously vortexing for 10 min at room temperature. After centrifugation at 3,000 rpm for 5 min, the supernatant was discarded, and the extraction step was repeated one more time. The acidic lipids were extracted by adding 0.5 mL MeOH:$CHCl_3$:12 M HCl (80:40:1) with continuous vortexing for 25 min at room temperature. Extracts were centrifuged at 3,000 rpm for 5 min, and the supernatant was transferred to a new 1.5 mL tube; 0.15 mL of $CHCl_3$ and 0.27 mL of 0.1 M HCl were added to the supernatant, vortexed, and centrifuged at 3,000 rpm for 5 min to separate organic and aqueous phases. The organic (lower) phase 0.3 mL was transferred into a new vial for PIP3 measurement. All the samples were dried for 4 h at 4°C. PIP3 samples were resuspended in 125 µL of PBS-Tween+3% Protein Stabilizer (provided by the Echelon kit). Samples were sonicated in an ice-water bath for 5 min, vortexed, and spun down before being added to the ELISA. All experiments were performed three times, each performed in triplicate. The lipid amount (60 µL) was used and was always run twice for each sample. After color reaction for 30 min in the dark, the 96-well plate was read by measuring the absorption at 450 nm with the SpectraMax M5 (Molecular Device). PIP3 concentrations were determined using GraphPad Prism software (version 6.0; GraphPad Software Inc., San Diego, CA).

Statistical analysis

All data are shown as the mean ± standard error of the mean (SEM). Statistical comparisons were made using GraphPad Prism 6 (GraphPad Software Inc., San Diego, CA) or Excel-Toukei 2012 software (Social Survey Research Information Co. Ltd., Osaka, Japan). Paired or Student's *t*-tests were used to compare two groups, and one-way ANOVA with Tukey's multiple comparison test or Dennett's multiple comparison test for more than two groups. Differences were considered statistically significant at $p < 0.05$.

Declarations

Acknowledgements

We are grateful to the Institute of Comprehensive Medical Research, Division of Animal Research Promotion Division (Aichi Medical University) for maintaining the mice, providing advanced research promotion for the expression analysis of genes and proteins, and performing measurements of cAMP, fluorescence, and phagocytosis. This study was supported by the JSPS KAKENHI (Grant Number 19K09962), the 24th General Assembly of the Japanese Association of Medical Sciences, Terumo Life Science Foundation, Takeda Science Foundation, Suzuken Memorial Foundation, Kato Memorial Bioscience Foundation, and the UBE Foundation.

Author contributions:

Conceptualization, K.I.; Methodology, K.I.; Investigation, K.I.; Writing – Original Draft, K.I.; Writing – Review & Editing, K.I., and S.M.; Funding Acquisition, K.I.; Resources, K.I., and S.M.; Supervision, K.I., and S.M.

Conflict of interest

The authors declare that they have no conflicts of interest.

References

1. Ralph, M. R., Foster, R. G., Davis, F. C. & Menaker, M. Transplanted suprachiasmatic nucleus determines circadian period. *Science* **247**, 975–978 (1990).
2. Mohawk, J. A., Green, C. B. & Takahashi, J. S. Central and peripheral circadian clocks in mammals. *Annual Review of Neuroscience* **35**, 445–462 (2012).
3. Szabadi, E. Functional organization of the sympathetic pathways controlling the pupil: Light-inhibited and light-stimulated pathways. *Frontiers in Neurology* **9**, 1069 (2018).
4. Kalsbeek, A. & Fliers, E. Daily Regulation of Hormone Profiles. in *Circadian Clocks* (eds. Kramer, A. & Merrow, M.) 185–226 (Springer Berlin Heidelberg, 2013).
5. Bergeå, B., Bodin, L. & Svedbergh, B. Impact of intraocular pressure regulation on visual fields in open-angle glaucoma. *Ophthalmology* **106**, 997–1004 (1999).
6. Liu, J. H. K. *et al.* Nocturnal elevation of intraocular pressure in young adults. *Investigative Ophthalmology and Visual Science* **39**, 2707–2712 (1998).
7. Tsuchiya, S., Higashide, T., Toida, K. & Sugiyama, K. The Role of beta-adrenergic receptors in the regulation of circadian intraocular pressure rhythm in mice. *Current Eye Research* **42**, 1013–1017 (2017).
8. Tsuchiya, S., Buhr, E. D., Higashide, T., Sugiyama, K. & Van Gelder, R. N. Light entrainment of the murine intraocular pressure circadian rhythm utilizes non-local mechanisms. *PLoS ONE* **12**, 1–12 (2017).

9. Agnifili, L. *et al.* Circadian intraocular pressure patterns in healthy subjects, primary open angle and normal tension glaucoma patients with a contact lens sensor. *Acta Ophthalmologica* **93**, e14–e21 (2015).
10. Renard, E. *et al.* Twenty-four hour (nyctohemeral) rhythm of intraocular pressure and ocular perfusion pressure in normal-tension glaucoma. *Investigative Ophthalmology and Visual Science* **51**, 882–889 (2010).
11. Mansouri, K., Weinreb, R. N. & Liu, J. H. K. Effects of aging on 24-hour intraocular pressure measurements in sitting and supine body positions. *Investigative Ophthalmology and Visual Science* **53**, 112–116 (2012).
12. Grippo, T. M. *et al.* Twenty-four-hour pattern of intraocular pressure in untreated patients with ocular hypertension. *Investigative Ophthalmology and Visual Science* **54**, 512–517 (2013).
13. Braslow, R. A. & Gregory, D. S. Adrenergic decentralization modifies the circadian rhythm of intraocular pressure. *Investigative Ophthalmology and Visual Science* **28**, 1730–1732 (1987).
14. Yoshiromi, T. & Gregory, D. S. Ocular adrenergic nerves contribute to control of the orcadian rhythm of aqueous flow in rabbits. *Invest Ophthalmol Visual Science* **32**, 523–528 (1991).
15. Larson, R. S. & Brubaker, R. F. Isoproferenol stimulates aqueous flow in humans with Horner's syndrome. *Investigative Ophthalmology and Visual Science* **29**, 621–625 (1988).
16. Sujino, M. *et al.* Differential entrainment of peripheral clocks in the rat by glucocorticoid and feeding. *Endocrinology* **153**, 2277–2286 (2012).
17. Tsuchiya, S., Sugiyama, K. & Van Gelder, R. N. Adrenal and glucocorticoid effects on the circadian rhythm of murine intraocular pressure. *Investigative ophthalmology & visual science* **59**, 5641–5647 (2018).
18. Maus, T. L., Young, W. F. & Brubaker, R. F. Aqueous flow in humans after adrenalectomy. *Investigative Ophthalmology and Visual Science* **35**, 3325–3331 (1994).
19. Ikegami, K., Shigeyoshi, Y. & Masubuchi, S. Circadian regulation of IOP rhythm by dual pathways of glucocorticoids and sympathetic nervous system. *Invest Ophthalmol Visual Science* **61**, 26 (2020).
20. Shigekuni, O., Toichiro, K. & I., R. S. Selective Destruction of the Pigmented Epithelium in the Ciliary Body of the Eye. *Science* **184**, 1298–1299 (1974).
21. Stamer, W. D. & Clark, A. F. The many faces of the trabecular meshwork cell. *Experimental Eye Research* **158**, 112–123 (2017).
22. Tamm, E. R. The trabecular meshwork outflow pathways: Structural and functional aspects. *Experimental Eye Research* **88**, 648–655 (2009).
23. Sit, A. J., Nau, C. B., McLaren, J. W., Johnson, D. H. & Hodge, D. Circadian variation of aqueous dynamics in young healthy adults. *Investigative Ophthalmology and Visual Science* **49**, 1473–1479 (2008).
24. Cameron Millar, J., Phan, T. N., Pang, I. H. & Clark, A. F. Strain and age effects on aqueous humor dynamics in the mouse. *Investigative Ophthalmology and Visual Science* **56**, 5764–5776 (2015).

25. Johnson, M. 'What controls aqueous humour outflow resistance?' *Experimental Eye Research* **82**, 545–557 (2006).
26. Gregory, D. S. Timolol reduces IOP in normal NZW rabbits during the dark only. *Investigative Ophthalmology and Visual Science* **31**, 715–721 (1990).
27. Mcmenamin, P. G., William, P., Lee, V., Grierson, I. & Grindlef, F. C. J. Giant Vacuoles in the Lining Endothelium of the Human Schlemm ' s Canal after Topical Timolol Maleate. *Investigative Ophthalmology and Visual Science* **24**, 339–342 (1983).
28. Zhang, X., Ognibene, C. M., Clark, A. F. & Yorio, T. Dexamethasone inhibition of trabecular meshwork cell phagocytosis and its modulation by glucocorticoid receptor β. *Experimental Eye Research* **84**, 275–284 (2007).
29. Matsumoto, Y., Bahler, C. K., Hann, C. R. & Johnson, D. H. Dexamethasone decreases phagocytosis in human trabecular meshwork. *Investigative Ophthalmology and Visual Science* **37**, 1902–1907 (1996).
30. Gosain, A., Muthu, K., Gamelli, R. L. & DiPietro, L. A. Norepinephrine suppresses wound macrophage phagocytic efficiency through alpha- and beta-adrenoreceptor dependent pathways. *Surgery* **142**, 170–179 (2007).
31. Fu, L., Lai, J. S. M., Lo, A. C. Y. & Shih, K. C. Induction of significant intraocular pressure diurnal fluctuation in rats using a modified technique of microbead occlusion. *International Journal of Ophthalmology* **11**, 1114–1119 (2018).
32. Bunker, S. *et al.* Experimental glaucoma induced by ocular injection of magnetic microspheres. *Journal of Visualized Experiments* 1–5 (2015). doi:10.3791/52400
33. van Zyl, T. *et al.* Cell atlas of aqueous humor outflow pathways in eyes of humans and four model species provides insight into glaucoma pathogenesis. *Proceedings of the National Academy of Sciences of the United States of America* **117**, 10339–10349 (2020).
34. Schmidt, M., Dekker, F. J. & Maarsingh, H. Exchange protein directly activated by cAMP (epac): A multidomain cAMP mediator in the regulation of diverse biological functions. *Pharmacological Reviews* **65**, 670–709 (2013).
35. Makranz, C., Cohen, G., Reichert, F., Kodama, T. & Rotshenker, S. cAMP cascade (PKA, Epac, adenylyl cyclase, Gi, and phosphodiesterases) regulates myelin phagocytosis mediated by complement receptor-3 and scavenger receptor-AI/II in microglia and macrophages. *Glia* **53**, 441–448 (2006).
36. Steininger, T. S., Stutz, H. & Kerschbaum, H. H. Beta-adrenergic stimulation suppresses phagocytosis via Epac activation in murine microglial cells. *Brain Research* **1407**, 1–12 (2011).
37. Swanson, J. A. Phosphoinositides and engulfment. *Cellular Microbiology* **16**, 1473–1483 (2014).
38. Nizami, S., Hall-Roberts, H., Warrier, S., Cowley, S. A. & Di Daniel, E. Microglial inflammation and phagocytosis in Alzheimer's disease: Potential therapeutic targets. *British Journal of Pharmacology* **176**, 3515–3532 (2019).
39. Schmidt, C. *et al.* Phosphoinositide 3-kinase γ mediates microglial phagocytosis via lipid kinase-independent control of cAMP. *Neuroscience* **233**, 44–53 (2013).

40. Canetti, C. *et al.* Activation of Phosphatase and Tensin Homolog on Chromosome 10 Mediates the Inhibition of FcγR Phagocytosis by Prostaglandin E 2 in Alveolar Macrophages. *The Journal of Immunology* **179**, 8350–8356 (2007).
41. Yoshitomi, T., Horio, B. & Gregory, D. S. Changes in aqueous norepinephrine and cyclic adenosine monophosphate during the circadian cycle in rabbits. *Investigative ophthalmology & visual science* **32**, 1609–1613 (1991).
42. Jain, A. *et al.* Effects of thailanstatins on glucocorticoid response in trabecular meshwork and steroid-induced glaucoma. *Investigative Ophthalmology and Visual Science* **54**, 3137–3142 (2013).
43. Yarangümeli, A. & Kural, G. Are there any benefits of Betoptic S (betaxolol HCl ophthalmic suspension) over other beta-blockers in the treatment of glaucoma? *Expert opinion on pharmacotherapy* **5**, 1071–1081 (2004).
44. Aronoff, D. M., Canetti, C., Serezani, C. H., Luo, M. & Peters-Golden, M. Cutting Edge: Macrophage Inhibition by Cyclic AMP (cAMP): Differential Roles of Protein Kinase A and Exchange Protein Directly Activated by cAMP-1. *The Journal of Immunology* **174**, 595–599 (2005).
45. Daaka, Y., Luttrell, L. M. & Lefkowitz, R. J. Switching of the coupling of the β2-adrenergic receptor to different g proteins by protein kinase A. *Nature* **390**, 88–91 (1997).
46. Borrás, T., Buie, L. K., Spiga, M. G. & Carabana, J. Prevention of nocturnal elevation of intraocular pressure by gene transfer of dominant-negative RhoA in rats. *JAMA Ophthalmology* **133**, 182–190 (2015).
47. Fujimoto, T., Sato-Ohira, S., Tanihara, H. & Inoue, T. RhoA Activation Decreases Phagocytosis of Trabecular Meshwork Cells. *Current Eye Research* **46**, 496–503 (2021).
48. Shim, M. S., Kim, K. Y. & Ju, W. K. Role of cyclic AMP in the eye with glaucoma. *BMB Reports* **50**, 60–70 (2017).
49. Alvarado, J. A., Murphy, C. G., Franse-carman, L., Chen, J. & Underwood, J. L. Effect of β-Adrenergic Agonists on Paracellular Width and Fluid Flow across Outflow Pathway Cells. *Investigative ophthalmology & visual science* **39**, 1813–1822 (1998).
50. Belmonte, C., Barrels, S. P., Liu, J. H. K. & Neufeld, A. H. Effects of Stimulation of the Ocular Sympathetic Nerves on IOP and Aqueous Humor Flow. *Investigative Ophthalmology* **28**, 1649–1654 (1987).
51. Khalilimeybodi, A., Daneshmehr, A. & Kashani, B. S. Ca2+-dependent calcineurin/NFAT signaling in β-adrenergic-induced cardiac hypertrophy. *General physiology and biophysics* **37**, 41–56 (2018).
52. Zhu, J., Wang, Y., Hu, Q., Yuan, R. & Ye, J. Rottlerin acts as a therapeutic in primary open-angle glaucoma by targeting the trabecular meshwork via activation of Rap1 signaling. *Pharmacological Research* **159**, 104780 (2020).
53. Zhavoronkov, A. *et al.* Pro-fibrotic pathway activation in trabecular meshwork and lamina cribrosa is the main driving force of glaucoma. *Cell Cycle* **15**, 1643–1652 (2016).
54. Qiu, H., Zhu, B. & Ni, S. Identification of genes associated with primary open-angle glaucoma by bioinformatics approach. *International Ophthalmology* **38**, 19–28 (2018).

55. Dobbs, P. C., Epstein, D. L. & Anderson, P. J. Identification of isoenzyme C as the principal carbonic anhydrase in human ciliary processes. *Investigative Ophthalmology and Visual Science* **18**, 867–870 (1979).
56. Matsusue, Y., Horii-Hayashi, N., Kirita, T. & Nishi, M. Distribution of corticosteroid receptors in mature oligodendrocytes and oligodendrocyte progenitors of the adult mouse brain. *Journal of Histochemistry and Cytochemistry* **62**, 211–226 (2014).
57. Tresguerres, M. *et al.* Bicarbonate-sensing soluble adenylyl cyclase is an essential sensor for acid / base homeostasis. *Proceedings of the National Academy of Sciences* **107**, 442–447 (2010).
58. Perreau-Lenz, S. *et al.* Suprachiasmatic control of melatonin synthesis in rats: Inhibitory and stimulatory mechanisms. *European Journal of Neuroscience* **17**, 221–228 (2003).
59. Scott, J. *et al.* Exchange protein directly activated by cyclic AMP (EPAC) activation reverses neutrophil dysfunction induced by β2-agonists, corticosteroids, and critical illness. *Journal of Allergy and Clinical Immunology* **137**, 535–544 (2016).
60. Komoto, S., Kondo, H., Fukuta, O. & Togari, A. Comparison of β-adrenergic and glucocorticoid signaling on clock gene and osteoblast-related gene expressions in human osteoblast. *Chronobiology International* **29**, 66–74 (2012).
61. Emorine, L. J. *et al.* Structure of the gene for human beta 2-adrenergic receptor: expression and promoter characterization. *Proceedings of the National Academy of Sciences* **84**, 6995–6999 (2006).
62. Nuñez, F. J. *et al.* Glucocorticoids rapidly activate cAMP production via Gαs to initiate non-genomic signaling that contributes to one-third of their canonical genomic effects. *FASEB Journal* **34**, 2882–2895 (2020).
63. Hernandez, M. R. *et al.* Glucocorticoid Target Cells In Human Outflow Pathway: Autopsy and Surgical Specimens. *Investigative ophthalmology & visual science* **24**, 1612–1616 (1983).
64. Ishida, A. *et al.* Light activates the adrenal gland: Timing of gene expression and glucocorticoid release. *Cell Metabolism* **2**, 297–307 (2005).
65. Drijfhout, W. J., Van Der Linde, A. G., Kooi, S. E., Grol, C. J. & Westerink, B. H. C. Norepinephrine release in the rat pineal gland: The input from the biological clock measured by in vivo microdialysis. *Journal of Neurochemistry* **66**, 748–755 (2010).
66. Copinschi, G. & Challet, E. Endocrine rhythms, the sleep-wake cycle, and biological clocks. in *Endocrinology: Adult and Pediatric* (eds. Jameson, J. L. & Groot, L. De) 147–173 (Elsevier, 2016).
67. Stehle, J. H. *et al.* A survey of molecular details in the human pineal gland in the light of phylogeny, structure, function and chronobiological diseases. *Journal of Pineal Research* **51**, 17–43 (2011).
68. Rommel, T. & Demisch, L. Influence of chronic β-adrenoreceptor blocker treatment on melatonin secretion and sleep quality in patients with essential hypertension. *Journal of Neural Transmission* **95**, 39–48 (1994).
69. Orzalesi, N., Rossetti, L., Invernizzi, T., Bottoli, A. & Autelitano, A. Effect of timolol, latanoprost, and dorzolamide on circadian IOP in glaucoma or ocular hypertension. *Investigative Ophthalmology and Visual Science* **41**, 2566–2573 (2000).

70. Johnson, M., McLaren, J. W. & Overby, D. R. Unconventional Aqueous Humor Outflow: A Review. *Experimental Cell Research* **158**, 94–111 (2017).

71. Ikegami, K. *et al.* Effect of expression alteration in flanking genes on phenotypes of St8sia2-deficient mice. *Scientific Reports* **9**, 1–11 (2019).

Figures

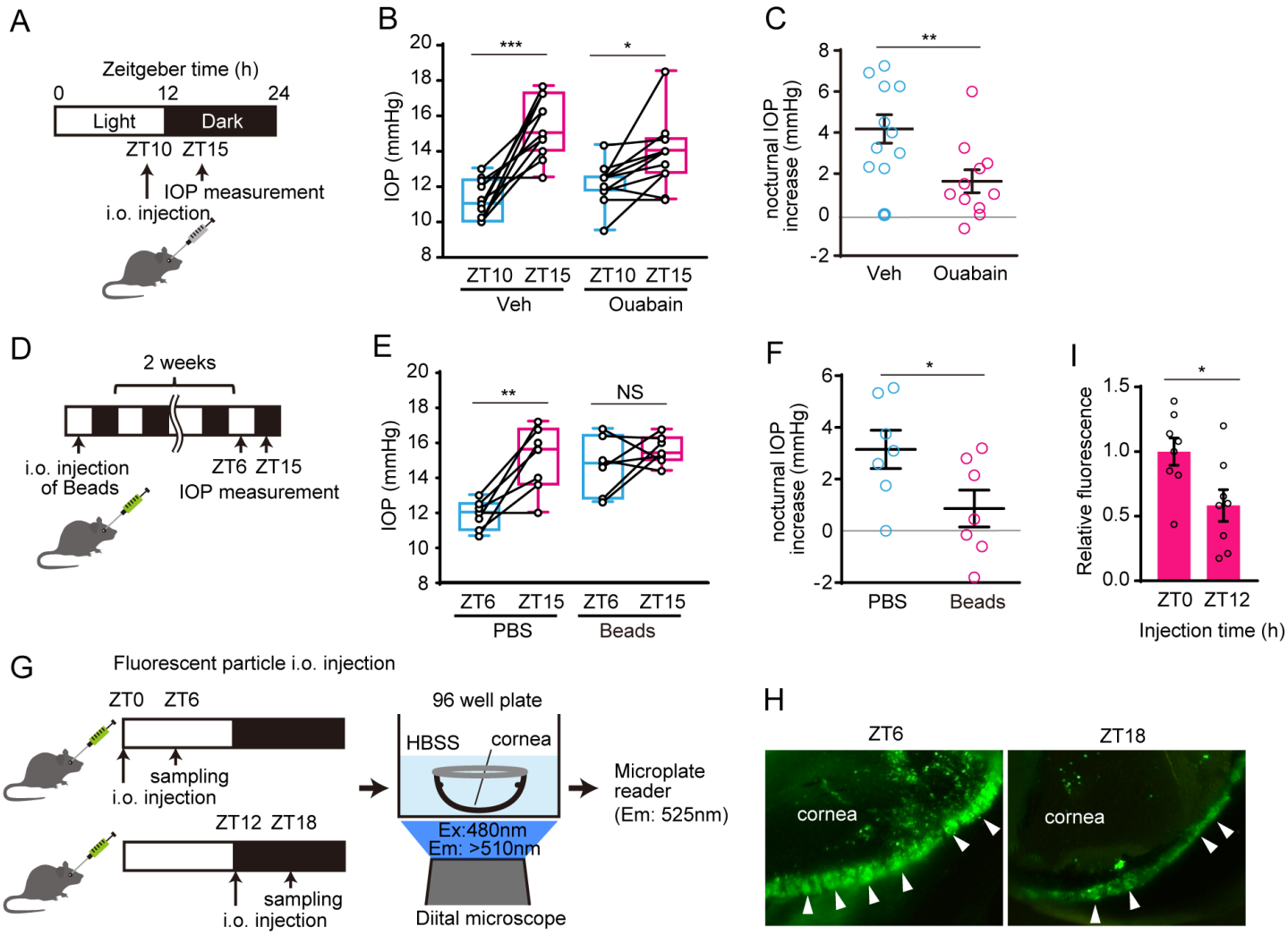

Figure 1

Day-time increase in aqueous humor outflow in mice. (A-C) Effect of Na+/K+ATPase antagonist, ouabain, treatment on nocturnal IOP increase. (A) Ouabain was injected to posterior chamber of mouse eye at ZT10, and IOP were measured before injection and 5 h after injection (ZT15). (B) Ouabain allowed a nocturnal IOP increase (paired t-test, ***p < 0.001, *p<0.05). Data are presented as box-and-whisker plots (n = 11). Variability is shown the box from the 25th to 75th percentiles, and min to max (whiskers). (C) Ouabain individually prevents a nocturnal IOP increase (t-test, **p < 0.01). Data are presented as scatter plots with mean ± sem (n = 11). (D-F) Diurnal changes of IOP (ZT6 and ZT15) were measured 2 weeks

after intraocular injection of beads. (E) IOP at ZT6 was increased up to nocturnal level (paired t-test, **p < 0.01). Data are presented as box-and-whisker plots (n = 7). (F) Day-night differences in individual IOP were arrested by bead injection. Data are presented as scatter dot plots with mean ± sem (n = 7). (G-I) Fluorescent particles were injected into the anterior chamber of the eye at ZT0 or ZT12, and after 6 h, the fluorescence of extracted cornea was observed with a microscope (Ex: 480 nm, Em: >510 nm) and quantified by microplate reader (Em: 525 nm). (H) Diurnal change of the particles at the edge of cornea (speculating the TM) was detected (arrowhead). (I) Fluorescent intensity at ZT6 was significantly higher than that at ZT18 (t-test, *p<0.05). Data are presented as scatter plots with mean ± sem (n = 8). ZT, Zeitgeber time.

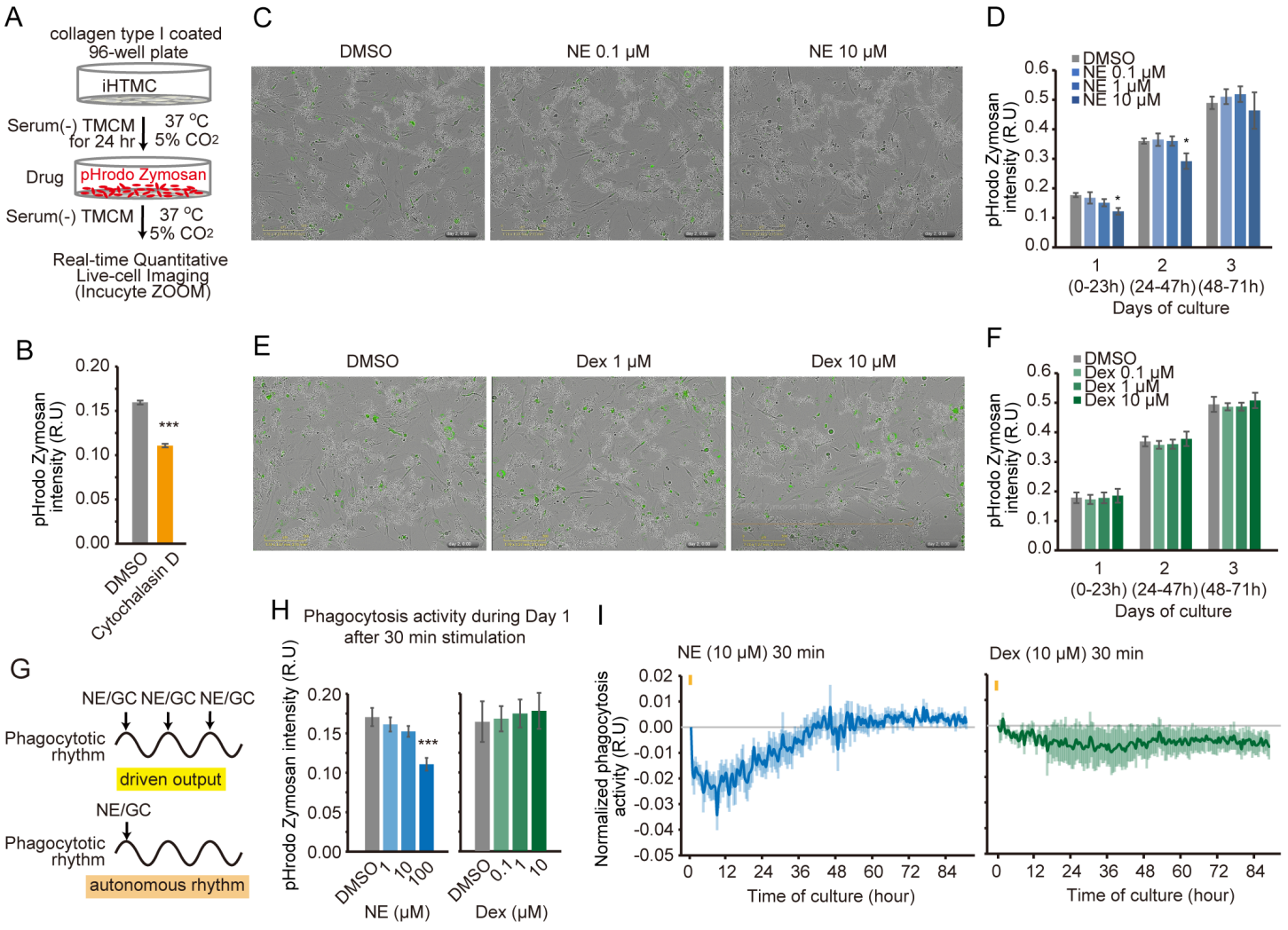

Figure 2

Driven-output stimuli of norepinephrine may suppress phagocytosis in iHTMC. (A) Immortalized human TM cells (iHTMC) were placed on type I collagen coated plates, and after 24 h, pH sensitive pHrodo Zymosan was added with norepinephrine (NE) and dexamethasone (Dex) to evaluate phagocytosis in real time over 3 days. (B) This ability was confirmed by phagocytosis inhibitor, cytochalasin D (t-test, ***p < 0.001). Mean ± SEM, n = 3 independent experiments. (C-F) Representative images 24 h after medium

changes including NE or Dex (0.1, 1, and 10 μM) (C, E), and quantified phagocytic activity (D, F). Scale bar = 300 μm. Continuous NE treatments dose-dependently prevent phagocytic activity in iHTMC during 2 days of culture (*p < 0.05 vs. DMSO, one-way ANOVA [p < 0.01], Dunnett's multiple comparison) (D), but not Dex (F). (G) Driven output regulation or a self-sustainable regulation after a single stimulation in diurnal phagocytosis changes. (H, I) Exposure of NE (1, 10, and 100 μM) or Dex (0.1, 1, and 10 μM) stimulation for 30 min to iHTMC and real-time phagocytic activity was observed in iHTMC for 3 days. Although we did not observe any circadian phagocytosis rhythm in the normalized fluorescence signal, a high NE pulse stimulation (yellow bar; 10 μM) suppressed phagocytosis for about 1 day (***p < 0.001 vs. DMSO, one-way ANOVA [p < 0.001], Dunnett's multiple comparison) (H, I) and this was later restored up to normal level (I), but Dex pulse stimulation (yellow bar; 10 μM), did not modulate phagocytosis rhythm (H, I). Mean ± SEM, n = 3 independent experiments.

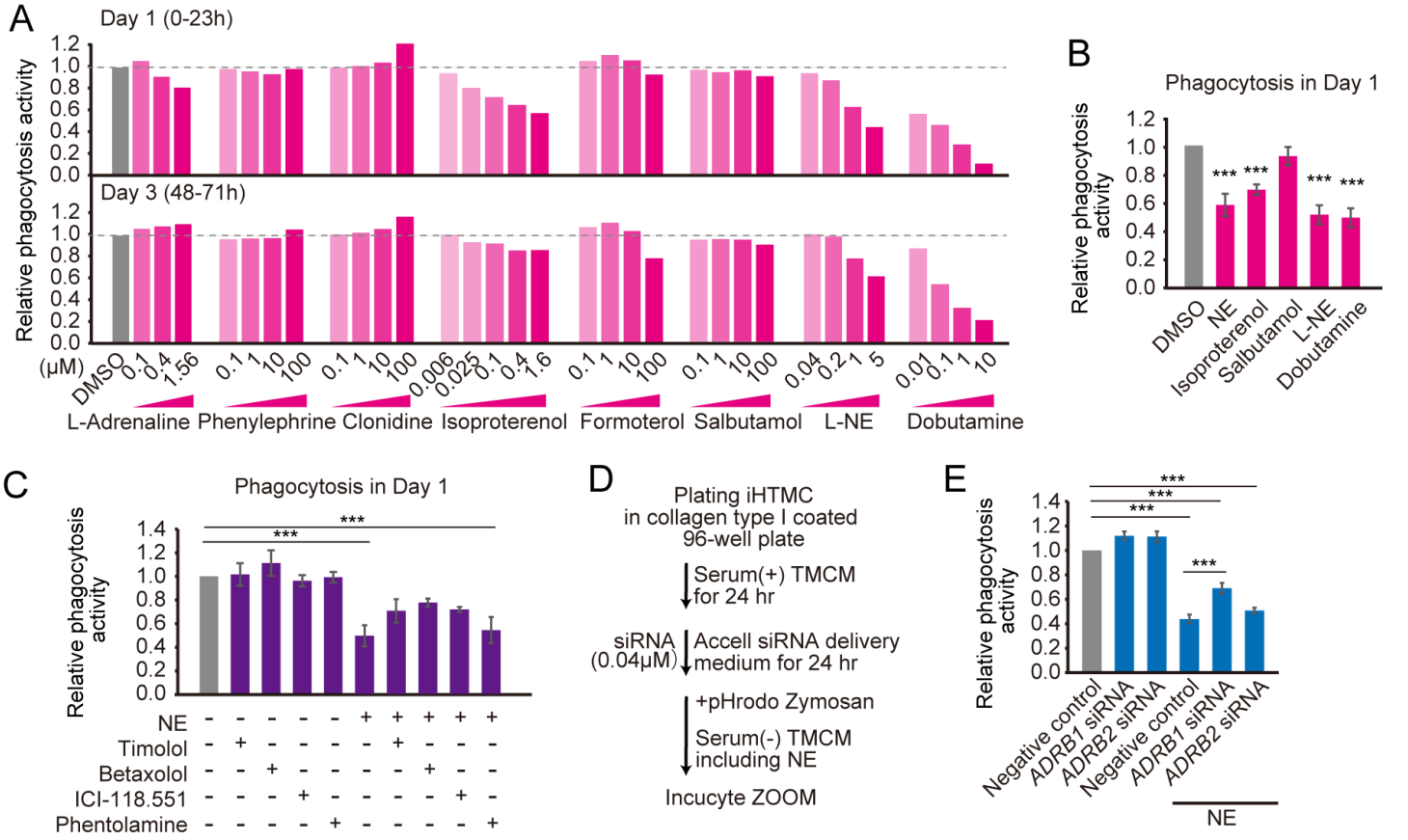

Figure 3

β1-adrenergic receptor (AR) mainly attenuated phagocytosis in iHTMC. (A) Effects of adrenergic receptor (AR) agonists on iHTMC phagocytosis for 3 days. Data shows mean (n = 1; quadruple experiment). Phagocytosis activities were normalized by control DMSO. Dose-dependent robust suppression of phagocytosis by AR-agonist L-adrenaline, β1-AR agonists (L-NE and dobutamine) and β1β2-AR agonist (isoproterenol) until 3 days, and no effect of selective α1-AR agonist (phenylephrine), direct-acting α2-AR agonist (clonidine), and β2-AR agonists (formoterol and salbutamol). (B) Detail analysis revealed the significant suppression of phagocytosis by L-NE, dobutamine, and isoproterenol as well as NE, but not by

β2-AR agonist salbutamol during day 1 (***p < 0.001 vs. DMSO, one-way ANOVA [p < 0.001], Dunnett's multiple comparison). Mean ± SEM, n = 3 independent experiments. (C) AR antagonists timolol (β1β2), betaxolol (β1), ICI-118.551 (β2) tended to rescue NE (5 μM)-suppressed normalized phagocytic activity but not phentolamine (α-AR antagonist) in iHTMC during day 1 (*p < 0.05, ***p < 0.001, one-way ANOVA [p < 0.001], Tukey's multiple comparison). Mean ± SEM, n = 3-4 independent experiments. (D) Timolol, betaxolol, and ICI-118.551 showed dose-dependent recovery effect. Data shows mean (n = 1; quadruple experiment). (E-F) Effect of RNA interference for β1β2-AR by siRNA against ADRB1 and ADRB2 on iHTMC phagocytosis. (E) After 24 h, siRNA (finally 0.04 μM) exposure with accell siRNA delivery medium, media were changed to those including NE (1 μM). (F) ADRB1 siRNA significantly increased phagocytic activity, but not ADRB2 siRNA (***p < 0.001, one-way ANOVA [p < 0.01], Tukey's multiple comparison). Mean ± SEM, n = 3-4 independent experiments.

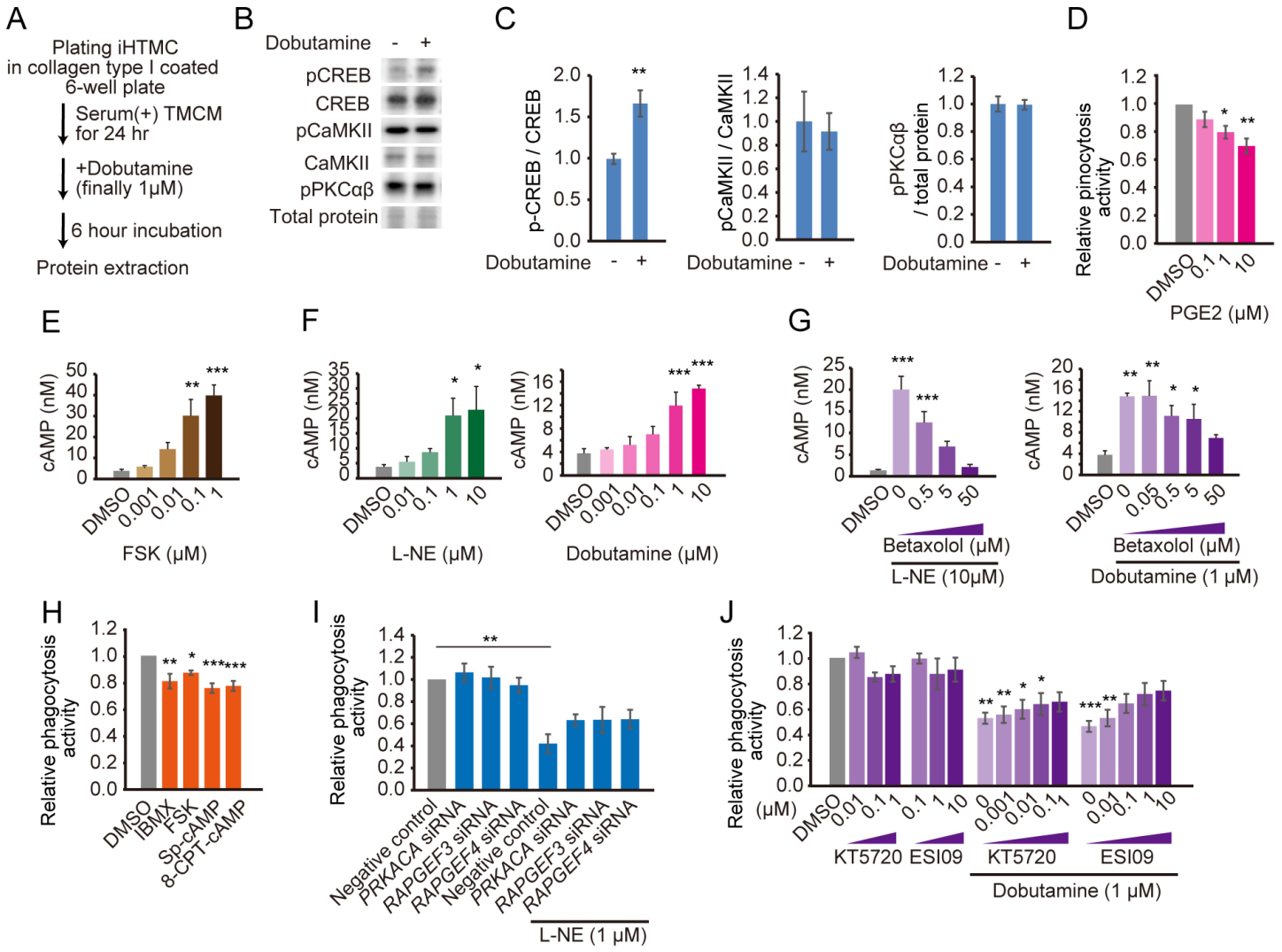

Figure 4

β1-AR mainly attenuated phagocytosis through cAMP-EPAC pathway. (A, B) Effect of 6-h dobutamine (1 μM) stimulation on GPCR-related signaling pathways. (B, C) Western blot analysis revealed that phosphorylated CREB (pCREB) (Gαi/Gαs-related maker) was increased by dobutamine (t-test, **p < 0.01),

but not phospho-CaMKII alpha (pCaMKII) (Gαq-related maker) and phospho-PKCα/βII [pPKCα/β] (Gαi/Gαq). Data are normalized by unphosphorylated protein or total protein and show mean ± SEM (n = 3 independent experiments). (D) Prostaglandin E2α (PGE2α), activating Gs-coupled GPCR, dose-dependently prevented iHTMC phagocytosis (*p < 0.05, **p < 0.01 vs. DMSO, one-way ANOVA [p < 0.001], Dunnett's multiple comparison). Mean ± SEM, n = 3 independent experiments. Phagocytosis activities were normalized to the control DMSO. (E, F) Dose-dependent intracellular cAMP accumulation by cAMP inducers forskolin (FSK)(E), and by L-NE and dobutamine (F). Mean + SEM, n = 3 independent experiments (*p < 0.05, **p < 0.01, ***p < 0.001 vs. DMSO, one-way ANOVA [p < 0.001], Dunnett's multiple comparison). (G) Betaxolol dose-dependently suppressed L-NE (10 μM)- or dobutamine (1 μM)-induced cAMP accumulation (*p < 0.05, **p < 0.01 vs. DMSO, one-way ANOVA [p < 0.001], Dunnett's multiple comparison). Mean + SEM, n = 3 independent experiments. (H) iHTMC phagocytic activity was slightly but significantly reduced by cAMP inducers (FSK and IBMX) and cAMP analogs, such as PKA activator Sp-cAMP and Epac/PKA activator 8-CPT-cAMP (*p < 0.05, **p < 0.01, ***p < 0.001 vs. DMSO, one-way ANOVA [p < 0.001], Dunnett's multiple comparison). Mean ± SEM, n = 3 independent experiments. Phagocytosis activities were normalized to the control DMSO. (I) siRNA (PRKACA, RAPGEF3, and RAPGEF4) administration significantly rescued β1-AR-mediated suppression of iHTMC phagocytosis (**p < 0.01, one-way ANOVA [p < 0.001], Tukey's multiple comparison). Mean ± SEM, n = 4 independent experiments. (J) The recovery effect of PKA and EPAC1/2 antagonists (KT5720 and ESI09, respectively) dose-dependently rescued dobutamine (1 μM)-suppressed iHTMC phagocytosis (*p < 0.05, **p < 0.01, ***p < 0.001 vs. DMSO, one-way ANOVA [p < 0.001], Tukey's multiple comparison).

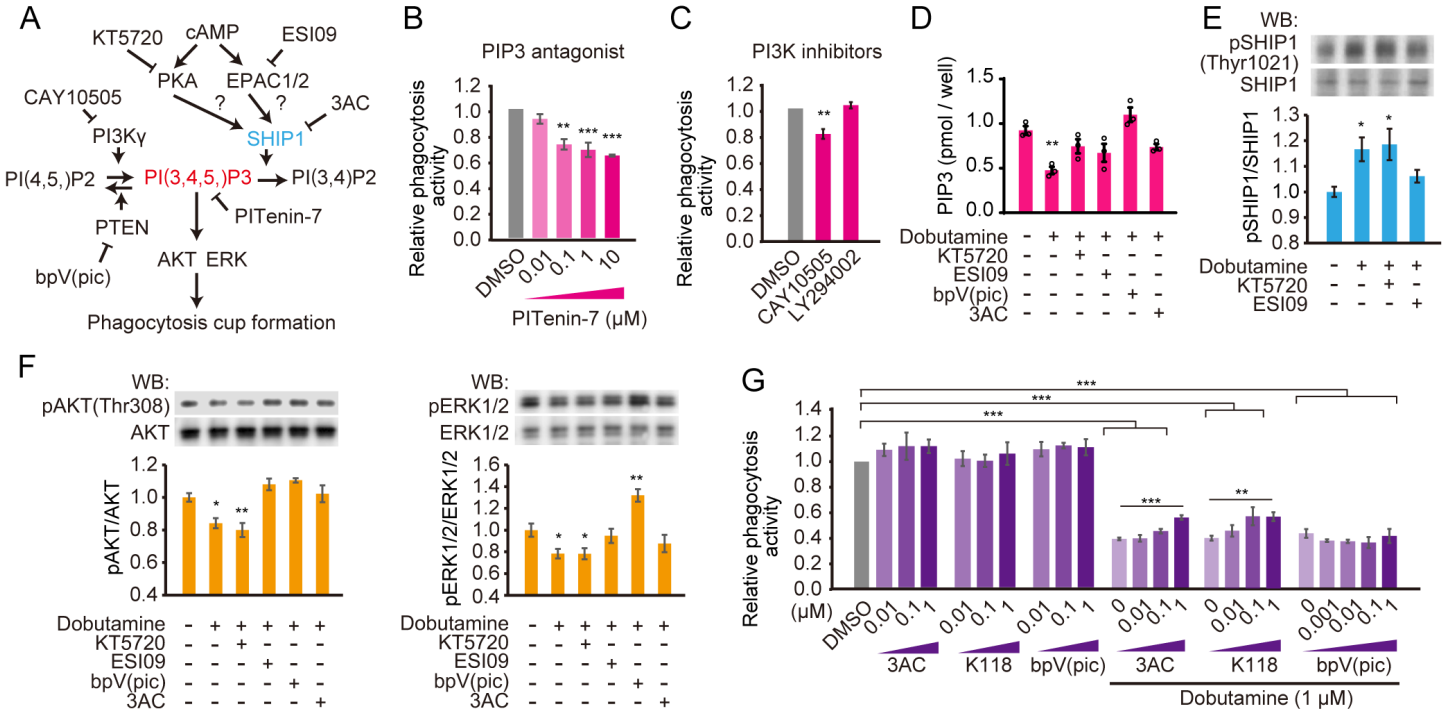

Figure 5

NE decreases PIP3 through SHIP activation via EPAC and PKA. (A) The hypothesized phagocytosis suppression mechanism by β1-AR-cAMP. PIP3 is a hub molecule to induce phagocytic cup formation through phosphorylation of AKT and ERK, and PI3K, PTEN, and SHIP1 regulate the level of PIP3. However, the involvement of EPAC and PKA in iHTMC in this system is unknown. (B) Administration of the PIP3 antagonist PITenin-7 dose-dependently and significantly suppressed the phagocytic activity of iHTMC (**p < 0.01, ***p < 0.001 vs. DMSO, one-way ANOVA [p < 0.001], Dunnett's multiple comparison). (C) Effect of LY294002 (inhibitor of PI3Kαβδ) and CAY10505 (selective PI3Kγ inhibitor) administration to iHTMC on phagocytosis (**p < 0.01 vs. DMSO, one-way ANOVA [p < 0.01], Dunnett's multiple comparison). (D) PIP3 levels after 6-h exposure to dobutamine with several antagonists in iHTMC. Dobutamine (1 μM) decreases PIP3, which are improved by KT5720 and ESI09. In addition, bpV (pic) (PTEN inhibitor) and 3AC (SHIP1 inhibitor) also improved it (**p < 0.01 vs. control, one-way ANOVA [p < 0.001], Dunnett's multiple comparison). Data are presented as scatter dot plots. (E) Western blot analysis of phosphorylation of SHIP1 in iHTMC. Dobutamine induced phosphorylated SHIP1, which was prevented by ESI09 but not KT5720 (**p < 0.01, ***p < 0.001 vs. DMSO, one-way ANOVA [p < 0.001], Dunnett's multiple comparison). Data are normalized to the unphospholylated SHIP1. (F) Involvement of the β1-AR signaling pathway in AKT or ERK1/2 phosphorylation. Dobutamine inhibited this phosphorylation, which was recovered significantly by ESI09, bpV (pic), and 3AC but not with KT5720 (*p < 0.05, **p < 0.01 vs. control, one-way ANOVA [p < 0.001], Dunnett's multiple comparison). Data are normalized by unphospholylated protein. (G) Recovery efficacy of bpV(pic), K118 (SHIP1 inhibitor), or 3AC on dobutamine (1 μM)-mediated phagocytosis suppression (**p < 0.01, ***p < 0.001, one-way ANOVA [p < 0.001], Tukey's multiple comparison). Phagocytosis activities were normalized to the control. Mean ± SEM, n = 3 independent experiments.

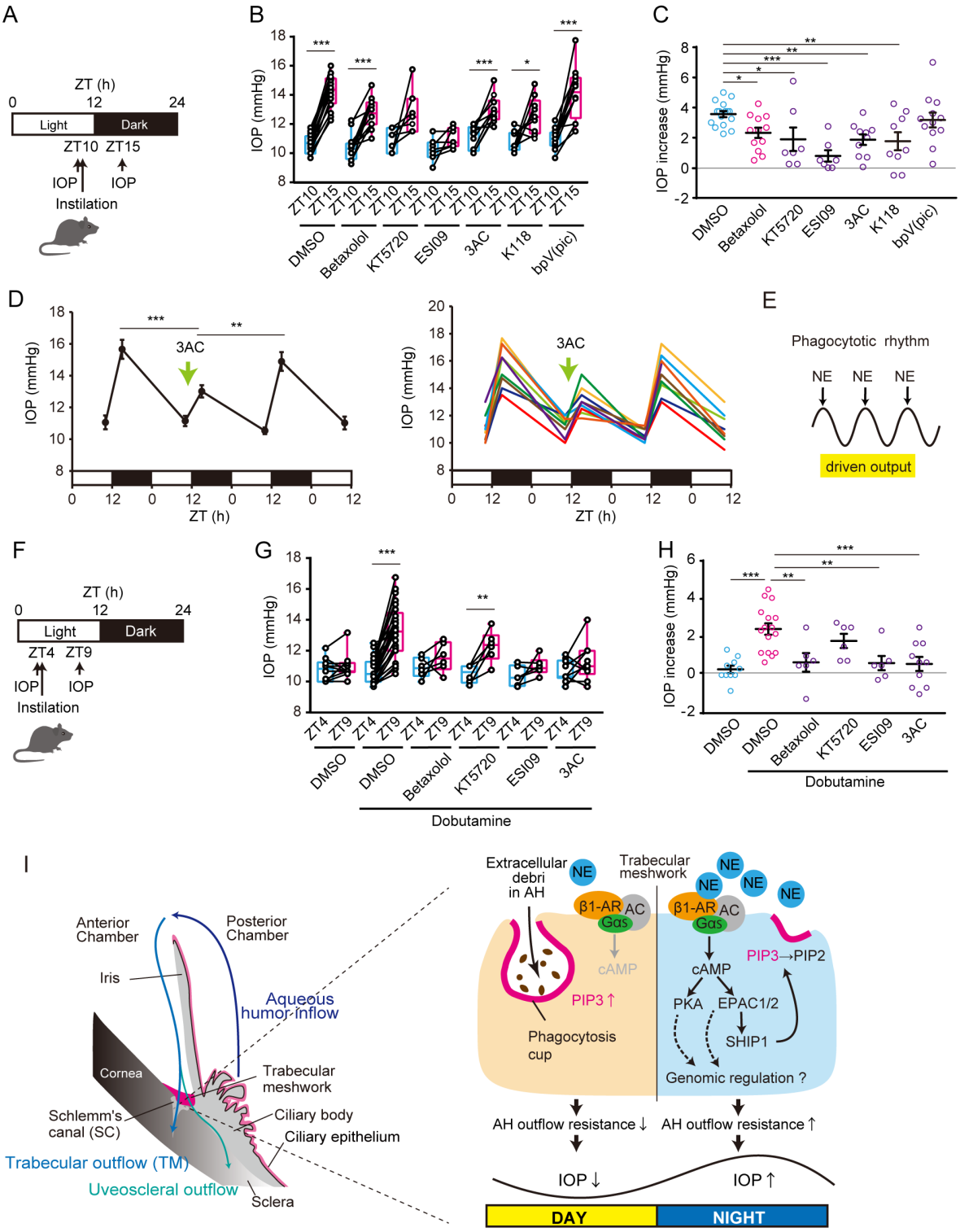

Figure 6

Nocturnal activation of the β1-AR-EPAC-SHIP1 pathway enhances IOP in mice. (A, B) Effect of β1-AR-EPAC-SHIP1 pathway-related inhibitors on nocturnal IOP increase in mice. Mice were administered an instillation of betaxolol (100 μM / 0.1% DMSO PBS), KT5720 (100 μM), ESI09 (100 μM), 3AC (1 mM), K118 (1 mM; SHIP1 inhibitor), and bpV(pic) (100 μM) at ZT10 and IOP were measured at ZT15. (B) Instillation with KT5720 and ESI09 significantly suppressed the nocturnal IOP increase (paired t-test, **p <

0.01, ***p < 0.001). Data are presented as box-and-whisker plots (n = 7-16). (C) All inhibitors except bpV (pic) prevented an IOP increase (*p < 0.05, **p < 0.01, ***p < 0.001 vs. DMSO, one-way ANOVA [p < 0.001], Dunnett's multiple comparison test). Data are presented as scatter plots with mean ± sem (n = 7-16). (D) Day-night changes of IOP one day before and after 3AC instillation. Data presented as mean ± sem (left; n = 10) and individual dynamics (right). At one day after single instillation, IOP showed normal nocturnal increase (**p < 0.01, ***p < 0.001, one-way ANOVA [p < 0.001], Bonferroni's multiple comparison test), providing (E) evidence of driven-output IOP enhancement by nocturnal NE. (F) Validation of IOP inhibitory effects of drugs on β1-AR-mediated IOP regulation using instillation of dobutamine (100 μM) at ZT4. After 5 hours, IOP was measured. (G, H) Dobutamine significantly enhanced the IOP, while preinstillation with betaxolol, ESI09, and 3AC prevented this profile (paired t-test, **p < 0.01, ***p < 0.001). Data are presented as scatter plots with mean ± sem (n = 6-16), and (H) the same was true for individual data (**p < 0.01, ***p < 0.001 vs. Dobutamine+DMSO, one-way ANOVA [p < 0.001], Dunnett's multiple comparison test). Data presented as (G) box-and-whisker plots and (H) scatter plots with mean ± sem (n = 6-16). (I) Regulatory model of time-dependent systems in which nocturnal NE suppresses phagocytosis to induce AH outflow resistance through β1-AR-EPAC-SHIP1 activation, leading to an IOP increase at night. The AH produced from the ciliary body is drained by two pathways; trabecular outflow and uveoscleral outflow.

Supplementary Files

This is a list of supplementary files associated with this preprint. Click to download.

- 20211029IOPrhythmTMikegamiNatCommunSupplymentalinformation.docx